Journal of Applied Physics ARTICLE pubs.aip.org/aip/jap

Physics of photovoltaic signal modifications in p–n photodiodes

Cite as: J. Appl. Phys. **134**, 174503 (2023); doi: 10.1063/5.0171614
Submitted: 9 August 2023 · Accepted: 8 October 2023 ·
Published Online: 3 November 2023

Mingrui Yuan,[1] Michael K. Rafailov,[2] and Rolf Binder[1,a)]

AFFILIATIONS

[1]Wyant College of Optical Sciences, University of Arizona, Tucson, Arizona 85721, USA
[2]Department of Chemical and Materials Engineering, University of Alberta, Edmonton, Alberta T6G 1H9, Canada

[a)]**Author to whom correspondence should be addressed:** binder@optics.arizona.edu

ABSTRACT

The photovoltaic signal is an important characteristic of photodetectors, including but not limited to those that are based on p–n or p–i–n photodiodes. In an open-circuit configuration, pulsed excitation of the detector with ultrafast (femto or nanosecond) pulses leads to a photovoltaic signal that decays slowly (micro-second time scale). If the physics in the detector is dominated by the recombination of the photo-excited charge carriers, one expects the signal to decay without changing its sign. However, some experiments using short-pulse excitation have found that photovoltaic signals can undergo a sign change as a function of time following excitation, with positive signals immediately following the excitation, turning to negative signals several microseconds later. Here, we study various physical effects (density, temperature, electrostriction, pressure, photostriction, and bandgap renormalization) and determine their effect on photovoltaic signals. If, following ultrafast excitation, the carrier density and temperature are increased, and during relaxation the system reaches a state sufficiently close to the quasi-thermal equilibrium in which the carrier density is still elevated, but smaller than the intrinsic thermal equilibrium density at the elevated temperature, then the signal can become negative.

I. INTRODUCTION

Photodetectors can transform light into electricity in optical power and communication systems, which are mainly based on the photovoltaic effect (Ref. 1) of semiconductor materials. The so-called photovoltaic effect refers to the phenomenon that light can create an electrical current or electrical voltage when it irradiates a suitably design material, such as a semiconductor p–n junction. The basic working mechanism of the photodetector includes three processes: (i) charge carriers are generated under illumination by light;[2] (ii) carrier drift and diffusion forms either transient or stationary electrical current in the photodetector;[3] and (iii) the photo-induced voltage or current is measured in an electrical circuit. In an open-circuit voltage configuration (e.g., Refs. 4–6 and p. 253 of Ref. 7), there is no electric current flowing under steady-state illumination. In the case of pulsed excitation, when the only physical process that is considered is charge-carrier recombination, the photovoltaic signal decays after excitation and is expected to remain positive over time. Some experiments using short-pulse excitation have found that photovoltaic signals can undergo a sign change as a function of time following excitation, with positive signals immediately following excitation, turning to negative signals after some time.[8–10]

Quite generally, we believe that high-excitation effects in photodiodes, either due to ultrafast pulsed excitation or due to strong stationary irradiation, are not well understood. While high-excitation effects like bleaching, density-induced dephasing, bandgap renormalization, heating, Auger recombination, etc., are well understood in spatially homogeneous semiconductors, in photodiodes, we have additional complication from carrier transport effects (drift and diffusion). This combination makes it difficult to associate a change in the measured signal to the underlying physics. In principle, highly excited photodiodes can have interesting microscopic processes. It it the purpose of this paper to use existing literature reporting experiments of highly excited photodiodes as a motivation to study theoretically how various physical processes affect the photovoltaic signal.

The experiment in Ref. 8 used an ultrashort (250 fs) pulse laser to excite a Ge p-i-n photodetector. They detected a sign change of the signal in the Ge photodetector (and in a similar Si-based photodetector) at approximately 50 μs after subpicosecond

excitation. The experiment in Ref. 9 investigated a HgCdTe n^+-on-p photodiode, which also showed a crossover on a μs time scale. Using a 20 ns laser pulse, they show a clear dependence of the crossover time (i.e., the time between optical excitation and the sign change of the photovoltaic signal) on the excitation power, with the crossover time increasing with increasing power. Reference 10 studied an InGaAs-InP p-i-n photodiode and found negative signals on a picosecond scale with sensitive dependence on the external bias and the excitation power.

Both Refs. 9 and 10 provide hypothetical explanations of the observed effects, but no theoretical analysis is given to support the hypotheses. Reference 9 explains the observed negative response in terms of temperature gradients combined with carrier diffusion that can be expected in their specific design geometry. Reference 10 briefly mentions a space-charge screening effect as a possible cause for the negative signal but does not elaborate on the detailed physical mechanism that could explain the observed effect.

There could be many reasons that lead to a negative signal, including instrument and electrical circuit effects. For example, using textbook I–V curves for photodetectors (e.g., p. 93 of Ref. 7), one can show that a simple circuit containing a photovoltaic detector (such as a p–n photodiode), a resistor, and a capacitor can give a transient negative signal after ultrafast photoexcitation.[11] On the other hand, the same simple circuit with a photoconductor instead of the photodiode does not give negative transient signals (more details in Ref. 11). Since those effects depend heavily on experimental details and are, therefore, not of fundamental importance, they will not be considered in this paper.

Instead, in this paper, we address the question of what kind of photovoltaic signal results from a given physical effect that can arise due to ultrafast optical excitation. To keep the analysis simple and general, we consider only a one-dimensional model (assuming the system to be spatially homogeneous in the other two dimensions). In other words, we do not consider possible complex space charge effects that would depend on the design details and geometry of a given photodiode. Furthermore, we restrict ourselves to the open-circuit voltage operation (e.g. p. 253 of Ref. 7). In our calculation, which is based on the self-consistent solution of Poisson's equation, we assume that the pn junction is in a stationary state (either in thermal equilibrium or quasi-thermal equilibrium where photo-excited electrons and holes are distributed according to Fermi functions in their respective bands). Our model also applies to slowly varying systems that, at each point in time, are approximately in the quasi-thermal equilibrium.

II. METHODOLOGY

A. Basic theory of p–n photodiode

We assume that the p–n diode extends from $z = -l/2$ to $z = l/2$, the p–n interface is $z = 0$, $z < 0$ is the p region, and $z > 0$ is the n region (Fig. 1).

The variables and constants used in this paper are summarized in Table I.

In order to analyze the photovoltaic effect, the voltage curve inside the photodiode, which contains the information of charge density, electric field, built-in voltage, and depletion region is necessary. The charge distribution must satisfy Poisson's equation, and

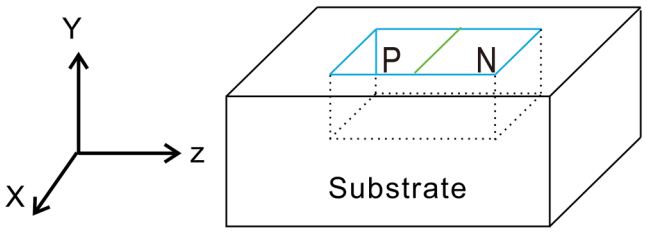

FIG. 1. Schematic p–n diode in open-circuit voltage configuration, no external voltage, no electrical leads or electrodes.

the voltage curve will be derived through this equation. Since doping is only z dependent, we will use the 1D Poisson's equation,

$$\begin{aligned} \frac{d}{dz}\epsilon_0\epsilon_b E(z) &= \rho(z) \\ \frac{d}{dz}V(z) &= -E(z), \end{aligned} \tag{1}$$

where $V(z)$ is the electric potential (voltage), $E(z)$ is the electrical field, $\rho(z)$ is the charge density, and $\epsilon_0\epsilon_b$ is the permittivity of Ge. The charge density should be determined from the charge carrier distribution functions as follows, where, again, we assume thermal or quasi-thermal equilibrium and, thus, use Fermi functions. The distribution function f_D of donors is

$$f_D(\mu_e, z) = \frac{1}{1 + \frac{1}{D_d} e^{\beta(U_c - \varepsilon_D - q_e V(z) - \mu_e)}}, \tag{2}$$

where U_c is the conduction band energy level; ε_D is the donor binding energy; q_e is the elementary charge; β is the the inverse temperature $1/k_B T$, where k_B is the Boltzmann constant; and D_d is the degeneracy of the donor states. The values of the parameters are listed in Table I. The z-dependent voltage $V(z)$ and electron chemical potential μ_e are to be determined. The charge density of

TABLE I. Parameters used in the numerical simulations.

Doping concentration of n and p-region, $N_D = N_A = 10^{17}$ (cm^{-3})
Elementary charge, $q_e = 1.60 \times 10^{-19}$ (C)
Effective mass of electron and hole, $m_e = m_h = 9.01 \times 10^{-31}$ (kg)
Length of light receiving area, $l = 6 \times 10^{-5}$ (cm)
Thickness of the p–n diode along y-direction, $d = 10^{-3}$ (cm)
Bandgap of Ge at 300 K and 0 Pa, $E_g = 0.66$ (eV)
Conduction band energy level, $U_c = 0.66$ (eV)
Valence band energy level, $U_v = 0$ (eV)
Acceptor binding energy, $\varepsilon_A = 10^{-3}$ (eV)
Donor band reduction, $\varepsilon_D = 10^{-3}$ (eV)
Thermodynamic beta, $\beta = 1/(k_B T)$
Degeneracy of the acceptor, donor states, D_a, $D_d = 2$
Vacuum permittivity, $\epsilon_0 = 8.85 \times 10^{-14}$ (F cm^{-1})
Relative permittivity of Ge, $\epsilon_b = 16.2$
Chemical potential of electrons and holes, μ_e, μ_h

ionized donor atoms [with $\theta(z)$ being the Heaviside step function] is

$$\rho_D(\mu_e, z) = q_e N_D[1 - f_D(\mu_e, z)]\ \theta(z). \tag{3}$$

The distribution function f_A of acceptors is

$$f_A(\mu_e, z) = \frac{1}{1 + \frac{1}{D_a} e^{\beta(U_v - \varepsilon_A + q_e V(z) - \mu_h)}}, \tag{4}$$

where U_v is the valance band energy level, $epsilon_A$ is the acceptor binding energy, D_a is the degeneracy of the acceptor states. The hole chemical potential is unknown. The charge density of ionized acceptor atoms,

$$\rho_A(\mu_h, z) = -q_e N_A[1 - f_A(\mu_h, z)]\ \theta(-z). \tag{5}$$

The density of electrons in the conduction band is

$$n_e(\mu_e, z) = \frac{2}{V_c} \sum_{\vec{k}} \frac{1}{1 + e^{\beta\left(\frac{\hbar^2 k^2}{2m_e} + U_c - q_e V(z) - \mu_e\right)}}, \tag{6}$$

where V_c is the volume of the p–n structure. The density of holes in the valance band is

$$n_h(\mu_h, z) = \frac{2}{V_c} \sum_{\vec{k}} \frac{1}{1 + e^{\beta\left(\frac{\hbar^2 k^2}{2m_h} + U_v + q_e V(z) - \mu_h\right)}}. \tag{7}$$

The total charge density is given by

$$\rho(\mu_e, \mu_h, z) = q_e(n_h(\mu_h, z) - n_e(\mu_e, z)) + \rho_D(\mu_e, z) + \rho_A(\mu_h, z). \tag{8}$$

B. Thermal equilibrium and quasi-thermal equilibrium

When there are no excited charges in the system, the system is in thermal equilibrium. The condition for the thermal equilibrium is

$$\mu \equiv \mu_e = -\mu_h \quad Q = 0, \tag{9}$$

where Q is the total charge density in the p–n diode,

$$Q = \frac{1}{l} \int_{-l/2}^{l/2} \rho(\mu_e, \mu_h, z) dz. \tag{10}$$

This can be rewritten as

$$\begin{aligned} \frac{1}{l} \int_{-l/2}^{l/2} n_e(\mu_e, z) dz &= N_e^{(0)}(T), \\ \frac{1}{l} \int_{-l/2}^{l/2} n_h(\mu_h, z) dz &= N_h^{(0)}(T), \\ \frac{1}{l} \int_{-l/2}^{l/2} \rho(\mu_e, \mu_h, z) dz &= 0, \end{aligned} \tag{11}$$

with $N_e^{(0)}(T) = N_h^{(0)}(T)$. We use the boundary condition

$$V(-l/2) = 0, \quad E(-l/2) = 0. \tag{12}$$

When there is excited charge in the system, we assume the system to be in the quasi-thermal equilibrium,

$$\mu_e \neq \mu_h \quad Q = 0. \tag{13}$$

The carrier right density after excitation is larger than the one in the thermal equilibrium,

$$\begin{aligned} \frac{1}{l} \int_{-l/2}^{l/2} n_e(\mu_e, z) dz &= N_e > N_e^{(0)}, \\ \frac{1}{l} \int_{-l/2}^{l/2} n_h(\mu_h, z) dz &= N_h > N_h^{(0)}, \\ \frac{1}{l} \int_{-l/2}^{l/2} \rho(\mu_e, \mu_h, z) dz &= 0. \end{aligned} \tag{14}$$

We use the same boundary condition as in the thermal equilibrium.

We define the energy difference between conduction band and μ_e as Δ_e and the energy difference between valance band and μ_h as Δ_h. Figure 2 is meant to clarify our nomenclature.

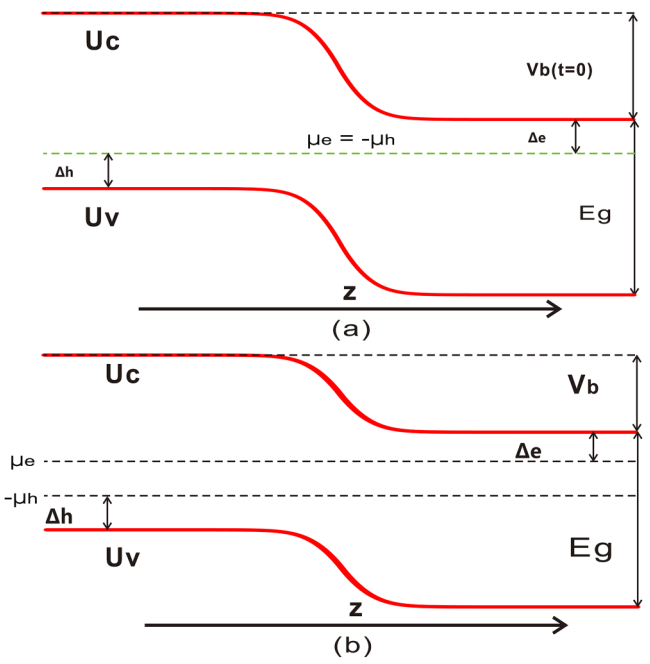

FIG. 2. Schematic z-dependent band profiles meant to clarify our definitions. (a) Thermal equilibrium and (b) quasi-thermal equilibrium.

As is shown in Fig. 2, the built-in voltage for thermal and quasi-thermal equilibrium cases can be expressed as

$$V_b = E_g + \Delta_e + \Delta_h - (\mu_e + \mu_h). \tag{15}$$

It shows that the built-in voltage varies with E_g, μ_e, μ_h, Δ_e, and Δ_h.

C. Hypothesis and framework

As mentioned above, the aim of our work is not to present a detailed microscopic simulation of a specific experiment, but a general study of the physical process that might contribute to a negative photovoltaic signal. However, our results are relevant for the existing experiments if the following conditions are fulfilled.

(i) The electronic system (charges) behaves essentially like a one-dimensional system (i.e., the charge distribution does not vary as a function of the transverse coordinates).

(ii) The system is in thermal or quasi-thermal equilibrium with zero macroscopic electrical current. For time-dependent systems, this implies that our study is restricted to a slow time scale where at each time the system has relaxed to its quasi-thermal state (see, e.g., Ref. 4).

(iii) The measured instantaneous photovoltaic signal is either the open-circuit voltage given as Eq. (7.14) on p. 185 of Ref. 12, here given in our nomenclature,

$$S_\mu = \mu_e + \mu_h \tag{16}$$

(note that $\mu_e + \mu_h = 0$ before excitation), or it is given by the photo-induced difference of the built-in voltage, which equals the photo-induced difference in the conduction band drop between the left and right terminals of the p–n junction,

$$S_b(t) = V_b(t = 0) - V_b(t) \tag{17}$$

The open circuit voltage refers ideally to the voltage difference between two terminals on a device when it is not connected to any external circuit and there is no current flowing through it (see, e.g., p. 24498 of Ref. 13). It can also be obtained from the I–V curve as the point where the current is zero[7,12] (see also Ref. 14). The built-in potential of the p–n photodiode, and hence, its modifications S_b can be measured, for example, by scanning Kelvin probe microscopy.[15,16] At a conceptual level, the advantage of S_b is that it involves only the electrostatic potential, which, in contrast to the chemical potentials, is well-defined even if the system is far from thermal or quasi-thermal equilibrium.

(iv) Transient effects related to the electrical circuit have been ruled out.

III. NUMERICAL SIMULATIONS

Here, we discuss results obtained from the numerical solution of the 1D Poisson equation.

For the thermal equilibrium state and room temperature, the total carrier concentration is found to be

$$\begin{aligned} N_e^{(0)}(300\,\mathrm{K}) &= \tfrac{1}{l}\int_{-l/2}^{l/2} n_e(\mu_e, V(z))dz = 4.07 \times 10^{16}\,\mathrm{cm}^{-3}, \\ N_h^{(0)}(300\,\mathrm{K}) &= \tfrac{-1}{l}\int_{-l/2}^{l/2} n_h(\mu_h, V(z))dz = 4.07 \times 10^{16}\,\mathrm{cm}^{-3}. \end{aligned} \tag{18}$$

After optical excitation, the whole system assumes a quasi-thermal equilibrium state, and the total number of charge carriers is increased,

$$N_e^{(0)} \overset{\text{Optical Excitation}}{\Longrightarrow} N_e \quad N_h^{(0)} \overset{\text{Optical Excitation}}{\Longrightarrow} N_h. \tag{19}$$

The carrier concentration change is

$$\Delta N = N_e - N_e^{(0)}(300\,\mathrm{K}) = N_h - N_h^{(0)}(300\,\mathrm{K}). \tag{20}$$

From the solution of the 1D Poisson equation, we find the built-in voltage and z-dependent voltage curves as they vary with N_e. In the quasi-thermal equilibrium state, the built-in potential decreases as N_e becomes larger. Figures 3 and 4 show how the carrier concentration changes the built-in voltage curve; larger the carrier concentration leads to smaller built-in potential. When there is no optical excitation, the built-in voltage is $V_{b(t=0)} \approx 0.374\,\mathrm{V}$. A simple curve fitting for the built-in potential vs carrier concentration change shows that there is an approximate exponential behavior of the form

$$V_b(N_e) \approx V_{b0}\, e^{-\frac{l}{w_0}\frac{N_e}{N_e^{(0)}(300K)}}, \tag{21}$$

where w_0 is the length of the depletion region without excitation.

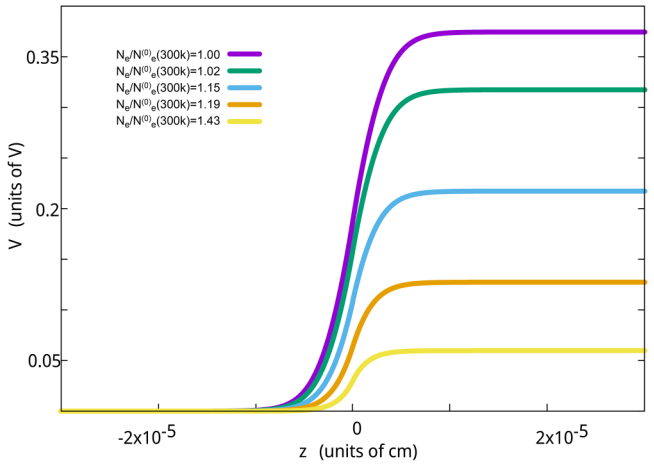

FIG. 3. Voltage curves for different total carrier concentrations.

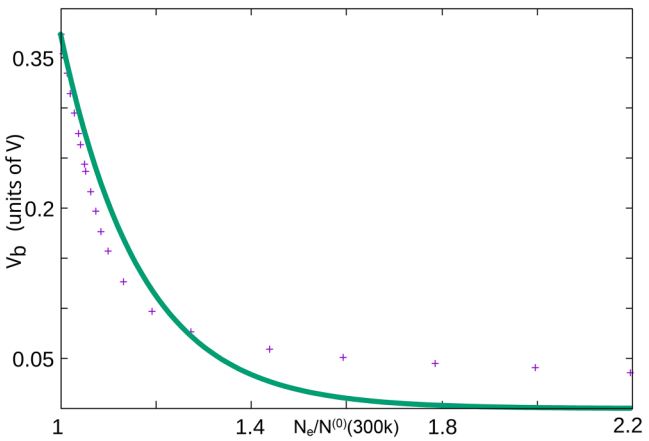

FIG. 4. Built-in potential vs carrier concentration change. Crosses from numerical results; green solid line from Eq. (21).

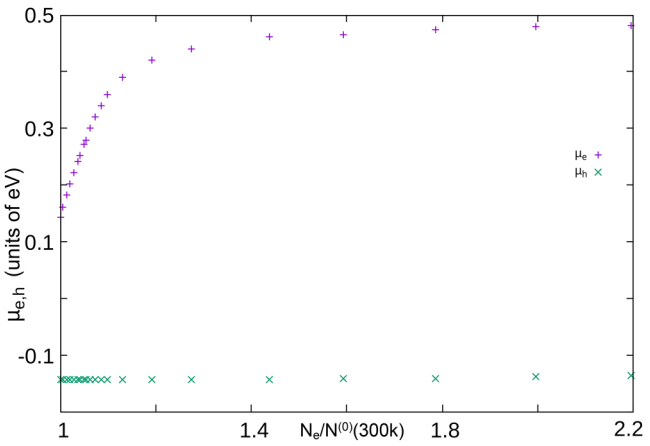

FIG. 6. Electron and hole chemical potential vs photo-induced carrier concentration.

Figure 5 shows the z-dependent charge density. As it should be, the length of the depletion region shrinks with increasing carrier concentration.

Based on the above results, the z-dependent band profile of the p–n photodiode can be constructed, which has the same shape as the flipping of the voltage curve.

In Fig. 6, we show that the optical excitation changes the chemical potentials, μ_e and μ_h. We note that due to the boundary condition, Eq. (12), μ_h is almost independent of the photo-induced carrier concentration, since it is energetically close to the top of the valence band at the left boundary, and since the electrostatic potential is chosen to be zero at the left boundary, the top of the valence band is independent of $V(z)$ at the left boundary. Based on the assumption 3 and Eq. (15), a reduction in the built-in potential leads to a negative signal. In Sec. IV, we will discuss the temperature, pressure, and other density effects related to built-in potential caused by the photo-excitation, and determine whether they lead to positive or negative signals.

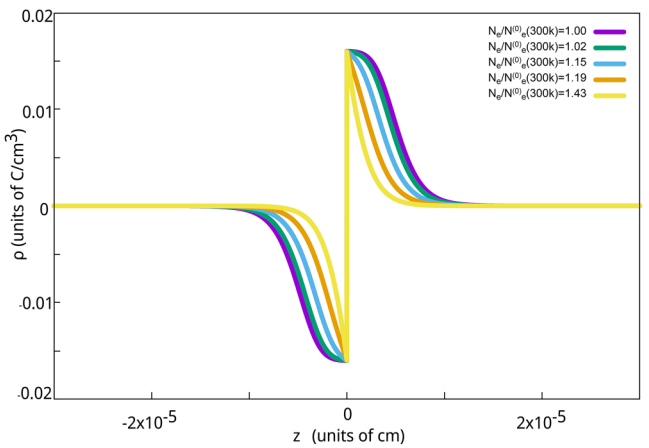

FIG. 5. Charge density vs z-coordinate.

IV. POTENTIAL EXPLANATIONS

In this section, we will introduce some potential explanations to the negative signal, and their corresponding symbols are shown in Table II.

A. Optical excitation without temperature increase

Figure 7 shows the signal obtained with the following effects (from Table II): optical excitation of the carrier density N_e and N_h (with $N_h = N_e$), bandgap renormalization $E_g(N_e, N_h)$, and photostriction (for details on bandgap renormalization and photostriction, see discussion in Secs. IV H and IV G, respectively, below). No change in temperature is taken into account in this figure. We see that in this case, the signals S_μ abd S_b are positive. We also note that without change of temperature and for the density range shown in this figure, the signals S_μ and S_b are almost equal in magnitude. For larger densities, S_b and S_μ become noticeably different.

TABLE II. Potential explanations and symbols.

Effect	Symbol
Only optical excitation	N_e, N_h
Only carrier heating	T, μ_e, μ_h
Only temperature-dependent bandgap reduction	$E_g(T)$
Only pressure increase (from anisotropic thermal expansion + constraints)	N_e, N_h $E_g(p)$
Only bandgap renormalization	$E_g(N_e, N_h)$
Only photostriction (expansion from increased density)	$E_g(N_e, N_h)$
Only electrostriction (polarization from strain)	Eq. (31)

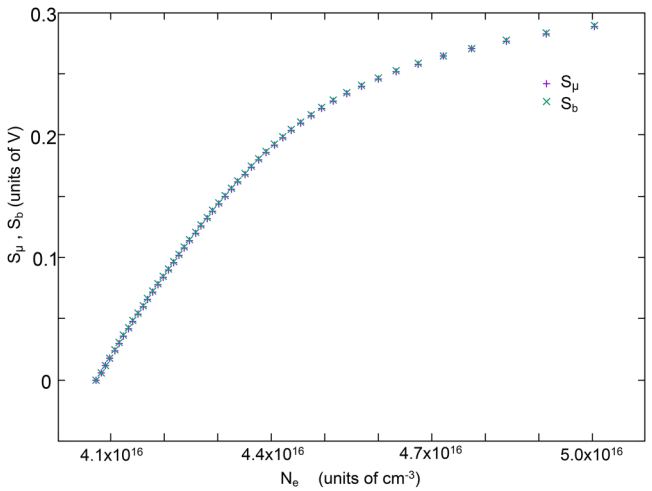

FIG. 7. The signals S_μ abd S_b (almost indistinguishable in this plot) as a function of excited carrier density at fixed temperature $T = 300$ K.

B. Electrostriction effect

Although the piezoelectric effect, i.e., the appearance of macroscopic electric charges or macroscopic electric polarizations in response to strain or stress, with the reversal of strain/stress leading to a reversal of induced electrical charges/polarizations, can only occur in crystals without inversion symmetry, the effect of electrostriction can occur in all crystals and dielectrics.

Under the action of the electric field, the medium undergoes a (possibly very small) mechanical deformation (Ref. 17). For different materials, the value of the electrostriction coefficient may vary by orders of magnitude. For ceramic material (3%Ca/PMN), the electrostriction coefficient is $\gamma \sim 10^{-18}\,\mathrm{m^2\,V^{-2}}$ (Refs. 18 and 19), but for silicon $\gamma \sim 10^{-22}\,\mathrm{m^2\,V^{-2}}$ (Ref. 20). In some literature, the electrostriction tensor M is often used instead of γ.

In textbooks and reviews, e.g., Ref. 21, the relationship between stress (σ) and strain (ϵ) tensors is shown to be

$$\sigma = C\,\epsilon, \tag{22}$$

$$\epsilon = S\,\sigma, \tag{23}$$

$$C = S^{-1}, \tag{24}$$

where C is the elastic stiffness tensor and S is the elastic compliance tensor. We can write these relations explicitly for the tensor elements as

$$\sigma_{ij} = \sum_{kl} C_{ijkl}\epsilon_{kl}, \qquad \epsilon_{ij} = \sum_{kl} S_{ijkl}\sigma_{kl}, \tag{25}$$

where the subscripts assume the values x, y, and z (the Cartesian coordinates).

However, Ref. 22 pointed out that the strain also depends on the electric field. The electrostriction tensor (γ) enters the tensor relations as follows:

$$\epsilon = S\sigma + \gamma EE, \tag{26}$$

$$D = \epsilon_0\epsilon_b E + \gamma E\sigma. \tag{27}$$

As mentioned in Ref. 22, the second term in Eq. (27) can be viewed as an E-field-assisted piezoelectric polarization P_{pz}. Without the E-field, Ge has a center of inversion and is, thus, not a piezoelectric material. Using Eqs. (24), (26), and (27), the piezoelectric polarization is obtained as

$$P_{pz} \equiv \gamma E\sigma = \gamma C(\epsilon - \gamma EE)E. \tag{28}$$

For the case of Germanium (Ge), the values of the electrostriction tensor elements given in Ref. 22 maybe to too large, see the discussion in Ref. 20. Since Si and Ge have similar crystal structures and, therefore, can be expected to have electrostriction tensors of similar order of magnitude, we use in this paper the values for the electrostriction tensor for Si, rather than Ge, given in Ref. 20. If, in the future, more reliable data for the electrostriction tensor in Ge become available, the following estimate should be updated. For an order-of-magnitude estimate, we consider the case $E_x = E_y = E_z \equiv E$, and since Ref. 20 does not give a value for γ_{yxyx}, we assume γ_{yxyx} and γ_{xxxx} to have the same order-of-magnitude. The cubic term in P_{pz} is (unit C is Coulomb)

$$P_{pz}^{cubic}(z) \sim (2\times 4\times 4)\gamma_{yxyx}\,C_{yxyx}\,\gamma_{yxyx}\,E_x\,E_y\,E_z = 1.68\times 10^{-31}(C\,cm\,V^{-3})\,E(z)^3. \tag{29}$$

The linear term is, assuming the strain has no shear component and $\epsilon_{xx} = \epsilon_{yy} = 10^{-5}$,

$$P_{pz}^{linear}(z) \sim 2\gamma_{yxyx}\,C_{yxyx}\,\epsilon_{xx}\,E_z \sim 3.74\times 10^{-14}(C\,cm^{-1}\,V^{-1})\,E(z). \tag{30}$$

The maximum electric field at the center of the p–n photodiode is, in our case, $E(z)_{\max} = 10^5\,\mathrm{V\,cm^{-1}}$. Then, the linear piezo-term will be the dominant one, and the first line of Eq. (1) can be modified as

$$\frac{d}{dz}(\epsilon_0\epsilon_b E(z) + P_{pz}(z)) = \rho(z,\mu). \tag{31}$$

Restricting ourselves to the dominant linear piezo term, we have

$$\frac{d}{dz}(\epsilon_0\epsilon_b E(z) + 2\gamma_{yxyx}\,C_{yxyx}\,\epsilon_{xx}E(z)) = \rho(z,\mu). \tag{32}$$

The estimate for our case then yields

$$2\gamma_{yxyx}\,C_{yxyx}\,\epsilon_{xx} \sim 3.74\times 10^{-19}(C\,cm^{-1}\,V^{-1}) \ll \epsilon_0\epsilon_b. \tag{33}$$

Since the piezoelectric polarization factor ($\gamma C\epsilon$) is far less than the permittivity of Ge, we will, henceforth, neglect electrostriction effects in the Ge p–n photodiode.

C. Bandgap change due to temperature increase

Temperature affects many properties of semiconductors, such as the bandgap, intrinsic carrier concentration, and lattice constant. In this section, the temperature effect will be discussed in detail (see also Ref. 4). In the following, we assume a light-induced temperature increase $\Delta T = 10\,\mathrm{K}$. From Ref. 23, we use the following relationship between the indirect bandgap (units eV) and temperature (units eV),

$$E_g(T) = 0.741 - 4.561 \times 10^{-4}\frac{T^2}{T+210}. \tag{34}$$

Considering only the influence of temperature on the bandgap, we find the relationship between built-in potential and the temperature shown in Fig. 8.

D. Bandgap change due compressive pressure

Thermal expansion also needs to be considered when the temperature of the crystal changes. When the external pressure is constant, the volume of most substances increases with increasing temperature rises and shrinks when the temperature decreases. The essence of the thermal expansion of solid materials can be attributed to the fact that the average distance between particles in the lattice structure increases with temperature. Therefore, the change in the lattice constant can represent the change of volume.

If, however, the temperature increases but external constraints prevent the lattice constant from increasing, this will then lead to compressive strain. It is compressive, because at the elevated temperature the lattice constant would be larger, but in reality the lattice constant is not changed and, hence, smaller compared to what it should be at the elevated temperature.

Since the bandgap is pressure dependent, we estimate how the temperature changes the bandgap through pressure,

$$\Delta T \rightarrow \mathrm{LatticeConstantChange} \rightarrow \mathrm{VolumeChange} \rightarrow \mathrm{Pressure} \rightarrow \mathrm{E_g change}.$$

We will explain this process in detail in the following. The lattice constant expansion coefficient at room temperature for Ge is given in Ref. 23,

$$\alpha(T \sim 300\,\mathrm{K}) = 6\ 10^{-6}\,\mathrm{K}^{-1}.$$

The lattice constant expansion along the horizontal direction without shear strain is (to simplify the notation used below, we replace the indices x, y, and z by 1, 2, and 3, respectively),

$$\epsilon_{22} = \epsilon_{33} = \alpha\,\Delta T. \tag{35}$$

The volume of the photodiode increases when the temperature increases, but we assume the hardness of the substrate and the material surrounding the photodiode to be infinitely large; therefore, the photodiode can only expand along the vertical direction. Therefore, as the temperature increases, horizonal compressive pressure builds up in the photodiode. Figure 9 shows this schematically. Therefore, only the top surface does not suffer from the pressure, and the pressure can be expressed from Eq. (25) as

$$\sigma_{11} = C_{11}\epsilon_{11} + C_{12}\epsilon_{22} + C_{13}\epsilon_{33} = 0. \tag{36}$$

Here, for convenience, we use the contracted form of elastic stiffness and elastic compliance tensors $C_{11} = C_{xxxx}$, $C_{12} = C_{xxyy}$, $C_{44} = C_{yzyz}$.

Based on the symmetry properties $C_{12} = C_{21} = C_{23} = C_{32}$, $C_{11} = C_{22} = C_{33}$, we have

$$\frac{\epsilon_{11}}{\epsilon_{22}} = -\frac{2\,C_{12}}{C_{11}} \approx -0.75. \tag{37}$$

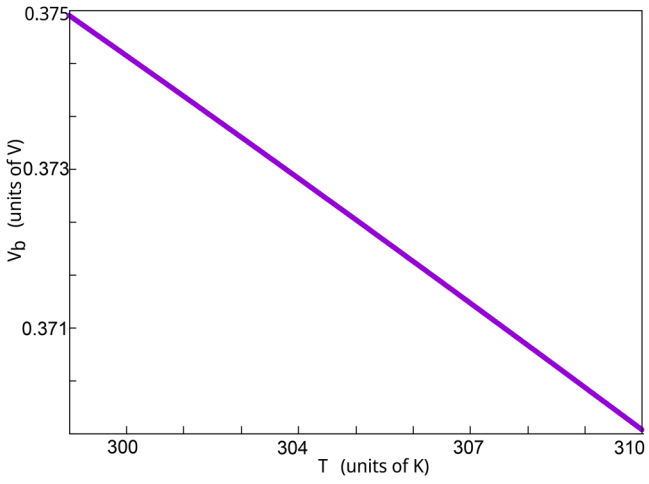

FIG. 8. The built-in potential vs temperature for the case that the temperature affects only the bandgap.

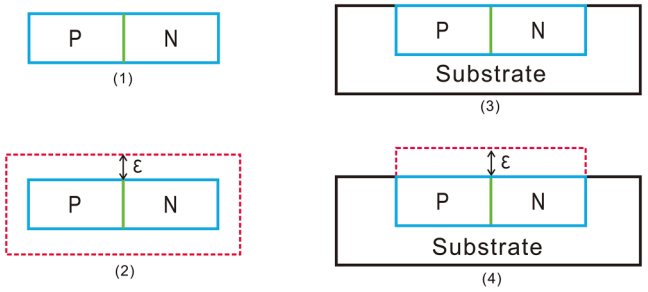

FIG. 9. (1) Schematic of the photodiode at room temperature, (2) the photodiode after thermal expansion in vertical and horizontal direction (red dashed line) without constraints, (3) the photodiode with substrate at room temperature, and (4) the photodiode with a substrate after thermal expansion in the vertical direction, but without thermal expansion in the horizontal direction.

The horizontal "backward pressure" is given by

$$\sigma_{33} = \sigma_{22} \equiv -\Delta p = C_{21}\epsilon_{11} + C_{22}\epsilon_{22} + C_{23}\epsilon_{33}. \tag{38}$$

The pressure dependence of the bandgap at room temperature is given in Ref. 24 [for silicon, this value is negative (Ref. 25)]:

$$\frac{\partial E_g}{\partial P} = 5.0 \times 10^{-11}\ \text{eV/Pa},$$
$$\Delta E_g = \frac{\partial E_g}{\partial p}\,\Delta p. \tag{39}$$

Considering only the influence of pressure on the bandgap, we find the relationship between the built-in potential and the temperature-induced pressure shown in Fig. 10.

E. Temperature and chemical potential

The temperature rise will also cause thermal excitation, which will increase the number of electrons and holes. We call this phenomenon carrier heating, by which we mean that we only change the temperature that explicitly enters the distribution functions [Eqs. (2) and (4)]. For example, when the temperature increases, the chemical potential or Δ_h, Δ_e will increase accordingly (in the solutions to the equations). The effect of thermal excitation on the built-in potential is shown in Fig. 11.

F. Total temperature effects

This subsection will summarize the bandgap effects discussed above. Figure 12 shows that the carrier heating and temperature bandgap change are the dominant effects. With an increase in the temperature, the built-in potential will decrease.

Note that temperature effects alone, without the effects of photo-excited carriers, change V_b and, therefore, lead to a signal S_b, but it does not yield a signal S_μ as long as the system stays in thermal equilibrium at the elevated temperature.

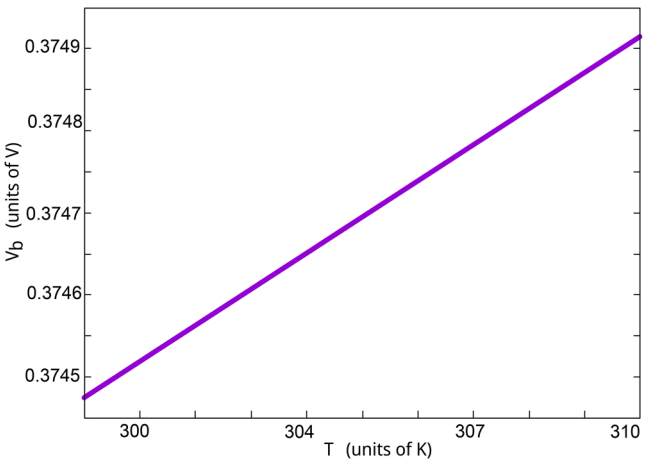

FIG. 10. The built-in potential vs temperature under the condition that the temperature induces only pressure effects that in turn modify the bandgap.

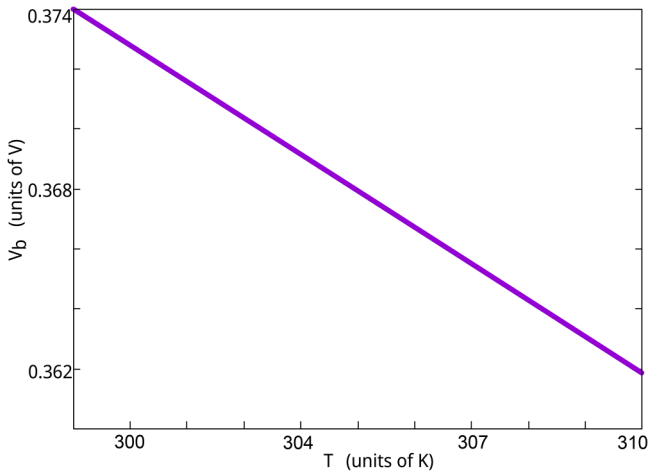

FIG. 11. The built-in potential vs temperature under the condition that only carrier heating.

G. Photostriction

Photostriction is the effect of changing the crystal volume as a consequence of changing the photo-induced carrier (electron-hole) concentrations. The basic definition of photostriction is that when excess carriers have been introduced into the sample by illumination, the lattice constant gets changed (crystal dilatation or expansion), see Refs. 26 and 27. Photostriction is useful in applications such as optical switches, tuneable lasers, and optical sensors. From

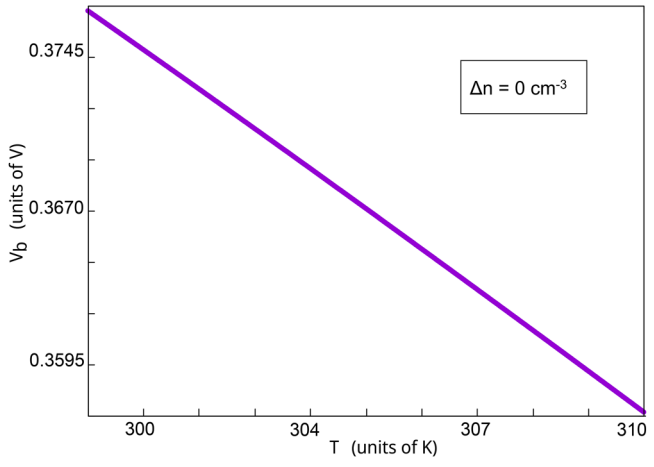

FIG. 12. The built-in potential vs temperature with all temperature effects included. For the parameters used here, the built-in voltage decreases with increasing temperature; hence, the photovoltaic signal is positive.

Refs. 24 and 28, the effect can be defined via

$$\frac{\delta V}{V} = \frac{dE_g}{dp}\Delta N. \tag{40}$$

For Ge, the pressure-dependent bandgap coefficient is

$$\begin{aligned}\frac{dE_g}{dp} &= 5 \times 10^{-6}\ \text{eV/bar} \\ &= 5 \times 10^{-6} \times 1.6\ 10^{-18}\ \text{cm}^3 = 8 \times 10^{-24}\ \text{cm}^3.\end{aligned} \tag{41}$$

When the extra carrier concentration is $\Delta N = 10^{17}\ \text{cm}^{-3}$, the volume expansion is

$$\frac{\delta V}{V} = 8 \times 10^{-24}\Delta N. \tag{42}$$

In Sec. IV D, we showed that, in our model, the expansion is only along the vertical direction. Therefore, the volume change can be expressed as the length change of the photodiode,

$$\begin{aligned}\frac{l\,l\,(d+\epsilon_{11})}{V} &= 1 + \frac{\delta V}{V}, \\ \epsilon_{11} &= \frac{\delta V}{V}.\end{aligned} \tag{43}$$

This is similar to the previous pressure effect, in that the photodiode only expands along the vertical direction. This effect also leads to the bandgap change. The horizontal "backward pressure" is given by

$$\sigma_{33} = \sigma_{22} = -\Delta p = C_{21}\epsilon_{11} + C_{22}\epsilon_{22} + C_{23}\epsilon_{33}. \tag{44}$$

The bandgap increases by

$$\Delta E_g = \frac{\partial E_g}{\partial p}\,\Delta p. \tag{45}$$

Considering only the influence of photostriction on the bandgap, we find the relationship between the built-in potential and the carrier as shown in Fig. 13.

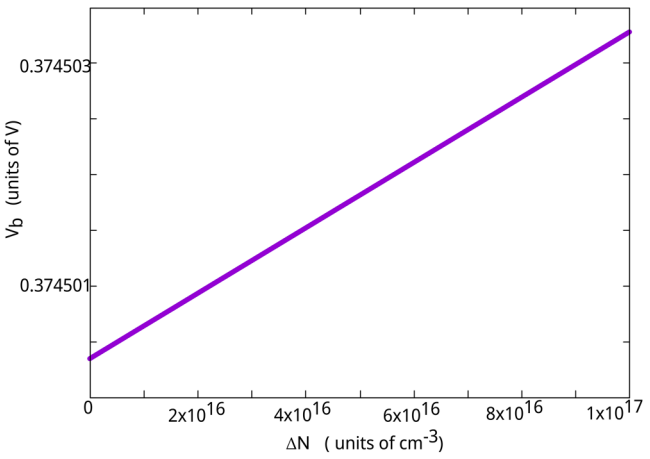

FIG. 13. The built-in potential vs photoinduced charge carrier density under the condition that the change in carrier concentration leads only to the photostriction effect, which in turn modifies the pressure-dependent bandgap.

H. Bandgap renormalization

Coulomb exchange interaction in the system of photo-induced charge carriers leads to the renormalization of electronic bands, here the valence and conduction bands, Ref. 29. Within the Hartree–Fock approximation, it is found that at the small electronic wave vector, this renormalization can be approximated as a rigid shift of the bands, i.e., the electronic self energies are approximately independent of the electronic wave vector. Under this condition, the effect of band renormalization is simply a change of the bandgap, i.e., bandgap renormalization (BGR). A useful analytical approximation for the BGR is given in Ref. 30,

$$\Delta E_g = -\frac{e^2\kappa}{2\epsilon_b}. \tag{46}$$

Here, κ is the 3D Thomas Fermi screening wave number,

$$\kappa = \sqrt{\frac{4\pi e^2 \Delta N \beta}{\epsilon_b}}. \tag{47}$$

Considering only the influence of bandgap renormalization on the bandgap, we find the relationship between the built-in potential and the carrier concentration change as shown in Fig. 14. The

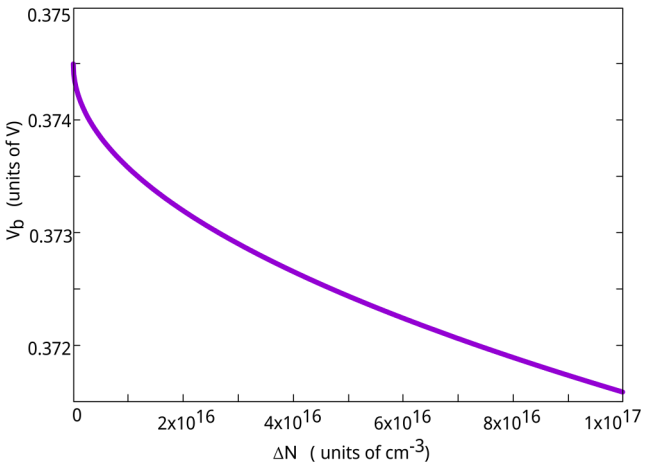

FIG. 14. The built-in potential vs photo-induced carrier concentration under the condition that the carrier concentration only leads to bandgap renormalization.

bandgap renormalization is the dominate effect, and it is several orders of magnitude larger than photostriction. With an increase in the carrier concentration, the built-in potential will decrease.

V. COMBINED CARRIER DENSITY AND TEMPERATURE INCREASE

In this section, we look at the case where the photodiode is excited with an ultrashort pulse, and then it relaxes back to the initial state. We assume that both the carrier density increase as a result of photo-excitation, and that also the temperature increases.

We again assume that all states involved in this process are quasi-thermal equilibrium states. This may not be true shortly after initial excitation but becomes more likely for the final phase of relaxation, which according to experiments can be on a microsecond time scale. Deviations from quasi-thermal equilibrium at long time scales may also depend on sample quality, as impurities and mid-gap states may hold localized or slowly diffusing carriers even on long time scales. The argument regarding a possible negative signal is limited to systems in or sufficiently close to the quasi-thermal equilibrium on long time scales. In Figs. 15 and 16, we plot signal S_μ and S_b, respectively, as a function of carrier density and temperature using quasi-thermal equilibrium. In this plane, the line $N_e^{(0)}(T)$ defines full thermal equilibrium (i.e., the function of intrinsic thermal carrier density vs temperature), at which $\mu_e + \mu_h = 0$ and, therefore, also $S_\mu = 0$. Point A is our initial state before optical excitation. It is reasonable to assume that excitation on a femtosecond time scale only changes the carrier density, not the temperature. Hence, immediately after ultrafast excitation, we would be at point B. The relaxation that follows will, in general, involve a temperature increase, for example, as a consequence of non-radiative recombination. Eventually, the system goes back to the starting point A. Hypothetical relaxation trajectories $N_e(t)$, $T(t)$, where t denotes time, are indicated in Fig. 15. The details of the trajectories depend on the details of the physical sample. But we can now distinguish between two different classes of relaxation trajectories, the ones that cross the thermal equilibrium line $N_e^{(0)}(T)$, and those who do not. Since the signal S_μ changes sign on the thermal equilibrium line, we conclude that a negative signal of S_μ occurs for the trajectories that cross the thermal equilibrium line.

We also see from Fig. 16 that the condition for a sign change of the signal S_b is more stringent. Not only does the trajectory have to cross the thermal equilibrium line, it also has to cross the $S_b = 0$ line at elevated temperature, which occurs at smaller densities.

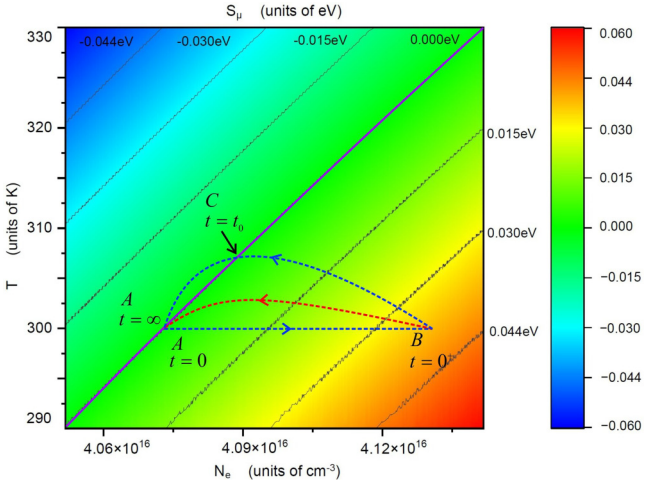

FIG. 15. The signal S_μ as a function of temperature and density. The family of diagonal lines are contour lines $S_\mu = constant$ with the constant value indicated. It is worth noting that the effects of small changes in bandgap (~0.05 eV) on S_μ can be neglected. The thick line is the thermal equilibrium line $N_e^{(0)}(T)$ at which $S_\mu = 0$; it separates positive (to the right of the line) from negative (left of line) signals. Also shown are two hypothetical trajectories (dashed lines): starting at point A, shortly are ultrafast optical excitation the density is increased but the temperature is still unchanged (point B), and the slow relaxation of density can be accompanied by a transient temperature increase. Depending on the details of the relaxation, trajectories may or may not cross the $S_\mu = 0$ line at point C. If they do and the system is indeed in quasi-thermal equilibrium, the signal becomes negative.

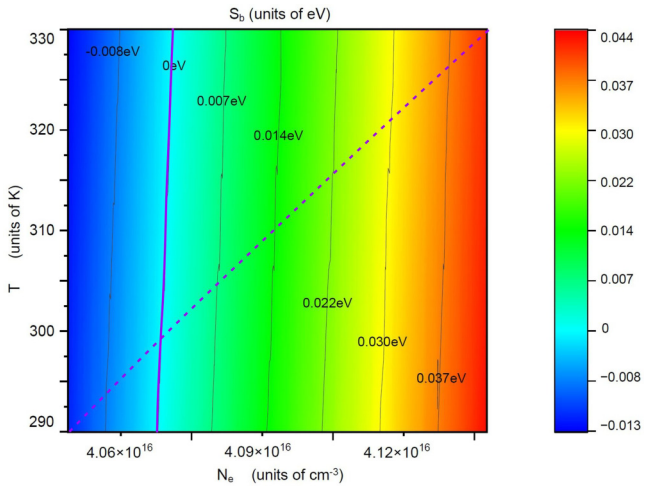

FIG. 16. This figure shows the signal S_b, which encompasses optical excitation of density, changes in bandgap resulting from temperature increase and compressive pressure, as well as contributions from temperature, chemical potential, and photostriction. The thick dashed line is the thermal thermal equilibrium line $N_e^{(0)}(T)$, and the thick (almost vertical) purple line shows where $S_b = 0$.

VI. CONCLUSIONS

We have studied several physical effects in p–n photodiodes and determined how these effects modify the photovoltaic signals S_μ [Eq. (7.14) on p. 185 of Ref. 12] and S_b (photo-induced difference in the built-in voltage). In addition to the strength of the signals, we determined their signs, i.e., whether the modification yields a positive or negative signal.

We restricted ourselves to the case of thermal and quasithermal equilibrium, and for the description of charge carrier effects, we restricted ourselves to a simple one-dimensional geometry of the p–n junction.

The restriction to the quasi-thermal equilibrium is valid if carrier recombination processes are slower than the equilibration of the carriers in their respective bands, i.e., the equilibration of electrons and holes before recombination, see e.g., p. 168 of Ref. 31. For example, in highly excited silicon (which, as germanium, is also an indirect-gap semiconductor), the intraband relaxation times can be as short as 10 fs,[32] which is similar to the case of direct-gap semiconductors.[33] Electron intraband relaxation due to coupling with acoustic and optical phonons takes place on a sub-picosecond time scale at room temperature.[34] Those time scales are well separated from that for interband transitions (carrier lifetimes), which have been found to be between 30 ns and 500 μs, see Ref. 35. Hence, our theory should be applicable to experiments that use ultrafast (fs or ps) optical excitations if the observation is limited to μs time scales. The theory is not valid on fs or ps time scales. It is also possible that quasi-thermal equilibrium is established locally, not, as we assume, globally. This could happen on a short (picosecond) time scale, on which fast intraband relaxation due to electron–electron and electron–phonon establishes a local quasi-thermal equilibrium, but carrier transport across the p–n junction may not have been completed. More important for our analysis would be spatial variations in the chemical potential and/or temperature on a long (microsecond) time scale. A possible reason for spatial variations on that time scale could be very slow diffusion of carriers in midgap states, which are not accounted for in our theory. This could affect the specific shape of the electrostatic potential and could, therefore, modify the measured signal. At each point in space, the basic trends related to various physical changes (e.g., temperature) can be expected to be the same as the ones found in our study, for example, if the temperature varies as a function of spatial coordinate z, the bandgap renormalization would vary accordingly with z. However, the net effect on the signal would have to be determined for each realization of the local quasi-thermal equilibrium, which in turn would need to be predicted by a drift-diffusion theory. Regarding the restriction to a one-dimensional geometry, we note that one-dimensional theories provide the most basic insight into the physics of p–n junctions and are, therefore, used in most textbooks (e.g., Refs. 7 and 12). Moreover, they have been successfully used to analyze experimental data of real photodiodes, see, e.g., Ref. 36.

For possible deformations (thermal expansion), we assumed the expansion to be limited to the direction perpendicular to the substrate. Our numerical approach includes the relation between photovoltaic signals and the bandgap and chemical potential. We analyzed several factors that affect the bandgap and chemical potential, in particular, photo-induced charges (i.e., increase in the carrier concentration), temperature change, and pressure changes caused by temperature increases.

If, on long times scales (toward the end of the relaxation), the system is sufficiently close to the quasi-thermal equilibrium and the relaxation trajectory in the plane of carrier density and temperature $(N_e(t), T(t))$ crosses the thermal-equilibrium line (i.e., the function of intrinsic thermal carrier density vs temperature) at an excitation-induced elevated temperature, then the signal S_μ becomes negative. A negative signal S_b has a more stringent condition; the relaxation trajectory has to cross the thermal equilibrium line and the line $S_b = 0$ at elevated temperatures.

Future research aimed at isolating strain-/stress-related effects may find that, in certain experimental configurations, the signal is negative. The strain-/stress-related effects that we found to give a negative signal in germanium-based photodiodes would not lead to a negative signal in silicon-based photodiodes, because the pressure coefficient of the bandgap has a different sign in Si; it is negative in Si while being positive in Ge.[28] It would also be interesting to study the effects of coherent phonons, as they can lead to substantial strain variations without necessarily involving a large temperature increase.

We also note that our study should only be considered a first step in analyzing the effect of strong optical excitation, be it ultrafast or stationary, in photodetectors (including photodiodes and photoconductors). In principal, each photodetector geometry can show different high-excitation effects, and possible sign changes or oscillations in the photovoltaic signal could hint at interesting physical effects happening at the microscopic level. Future research using a drift-diffusion approach, aimed at extending the analysis from the open-circuit voltage operation to the short-circuit current operation and at analyzing the effects of non-equilibrium transport phenomena, is desirable for further clarification of transient photodetector responses.

AUTHOR DECLARATIONS

Conflict of Interest

The authors have no conflicts to disclose.

Author Contributions

Mingrui Yuan: Conceptualization (equal); Formal analysis (equal); Methodology (equal); Software (lead); Writing – original draft (equal); Writing – review & editing (equal). **Michael K. Rafailov:** Conceptualization (equal); Writing – review & editing (equal). **Rolf Binder:** Conceptualization (equal); Formal analysis (equal); Methodology (equal); Supervision (lead); Writing – original draft (equal); Writing – review & editing (equal).

DATA AVAILABILITY

The data that support the findings of this study are available from the corresponding author upon reasonable request.

REFERENCES

[1]P. Rappaport, "The photovoltaic effect and its utilization," Sol. Energy **3**, 8 (1959).
[2]A. L. Linsebigler, G. Lu, and J. T. Yates, Jr., "Photocatalysis on TiO2 surfaces: Principles, mechanisms, and selected results," Chem. Rev. **95**, 735 (1995).
[3]B. Levine, "Quantum-well infrared photodetectors," J. Appl. Phys. **74**, R1 (1993).
[4]P. Löper, D. Pysch, A. Richter, M. Hermle, S. Janz, M. Zacharias, and S. W. Glunz, "Analysis of the temperature dependence of the open-circuit voltage," Energy Procedia **27**, 135 (2012).
[5]K. O. Hara and N. Usami, "Theory of open-circuit voltage and the driving force of charge separation in pn-junction solar cells," J. Appl. Phys. **114**, 153101 (2013).
[6]J. Wang, "Open-circuit voltage, fill factor, and heterojunction band offset in semiconductor diode solar cells," EcoMat **4**, e12263 (2022).

[7]E. Dereniak and G. Boreman, *Infrared Detectors and Systems*, A Wiley-Interscience publication (Wiley, 1996).
[8]I. Zakharova and M. K. Rafailov, "Detector response to high repetition rate ultra-short laser pulses. i," in *Micro-and Nanotechnology Sensors, Systems, and Applications VII* (SPIE, 2015), Vol. 9467, pp. 407–413.
[9]Z. Xu, J. Zhang, X. Lin, B. Shao, and P. Yang, "Negative response of hgcdte photodiode induced by nanosecond laser pulse," in *Fourth International Symposium on Laser Interaction with Matter* (SPIE, 2017), Vol. 10173, pp. 41–46.
[10]C.-K. Sun, I.-H. Tan, and J. E. Bowers, "Ultrafast transport dynamics of pin photodetectors under high-power illumination," IEEE Photonics Technol. Lett. **10**, 135 (1998).
[11]M. Yuan, "Physics of photovoltaic signal modifications in p-n photodiodes," Master's thesis (University of Arizona, 2023).
[12]P. Wuerfel and U. Wuerfel, *Physics of Solar Cells*, 3rd ed. (Wiley, Weinheim, 2016).
[13]T. Jirabovornwisut and A. Arpornwichanop, "A review on the electrolyte imbalance in vanadium redox flow batteries," Int. J. Hydrogen Energy **44**, 24485 (2019).
[14]I. M. Ikram, M. K. Rabinal, and B. G. Mulimani, "A laboratory experiment to measure the builtin potential of a pn junction by a photosaturation method," Eur. J. Phys. **30**, 127 (2008).
[15]C. S. Jiang, D. J. Friedman, H. R. Moutinho, and M. M. Al-Jassim, "Profiling the built-in electrical potential in III-V Multijunction solar cells," in *2006 IEEE 4th World Conference on Photovoltaic Energy Conference* (IEEE, 2006), Vol. 1, pp. 853–856.
[16]C. Jiang, H. Moutinho, D. Friedman, J. Geisz, and M. Al-Jassim, "Measurement of builtin electrical potential in III-V solar cells by scanning Kelvin probe microscopy," J. Appl. Phys. **93**, 10035 (2003).
[17]N. Astrath, B. Anghinoni, T. Pozar, I. Brevik, and S. Bialkowski, "Squeezing in on an electromagnetic controversy," Optics Photonics News **33**, 48 (2022).
[18]V. Sundar, J.-F. Li, D. Viehland, and R. Newnham, "Interferometric evaluation of electrostriction coefficients," Mater. Res. Bull. **31**, 555 (1996).
[19]S. Santucci and V. Esposito, "Electrostrictive ceramics and their applications," Encyclopedia Materials Technical Ceramics Glasses **3**, 369 (2021).
[20]S. W. Van Sterkenburg, "The electrostriction of silicon and diamond," J. Phys. D: Appl. Phys. **25**, 996 (1992).
[21]C. Kittel, *Introduction to Solid State Physics* (Wiley, 2004).
[22]A. A. Gundjian, "Electrostriction in germanium," Solid State Commun. **3**, 279 (1965).
[23]Y. P. Varshni, "Temperature dependence of the energy gap in semiconductors," Physica **34**, 149 (1967).
[24]W. B. Gauster, "Electronic dilation in germanium and silicon," Phys. Rev. **187**, 1035 (1969).
[25]E. Ghahramani and J. Sipe, "Pressure dependence of the band gaps of semiconductors," Phys. Rev. B **40**, 12516 (1989).
[26]T. Figielski, "Photostriction effect in germanium," Phys. Status Solidi B **1**, 306 (1961).
[27]S. Lee, W. Jo, A. D. DiChiara, T. P. Holmes, S. Santowski, Y. C. Cho, and E. C. Landahl, "Probing electronic strain generation by separated electron-hole pairs using time-resolved x-ray scattering," Appl. Sci. **9**, 4788 (2019).
[28]V. Chenniappan, G. Umana-Membreno, K. Silva, M. Martyniuk, A. Keating, J. Dell, and L. Faraone, "Photostriction actuation of silicon-germanium bilayer cantilevers," J. Appl. Phys. **125**, 125106 (2019).
[29]H. Haug and S. W. Koch, *Quantum Theory of the Optical and Electronic Properties of Semiconductors* (World Scientific, 2004).
[30]P. Vashishta and R. K. Kalia, "Universal behavior of exchange-correlation energy in electron-hole liquid," Phys. Rev. B **25**, 6492 (1982).
[31]H. Haug and S. W. Koch, *Quantum Theory of the Optical and Electronic Properties of Semiconductors*, 4th ed. (World Scientific, Singapore, 2004).
[32]B. E. Sernelius, "Intraband relaxation time in highly excited semiconductors," Phys. Rev. B **43**, 7136 (1991).
[33]R. Binder, D. Scott, A. E. Paul, M. Lindberg, K. Henneberger, and S. W. Koch, "Carrier-carrier scattering and optical dephasing in highly excited semiconductors," Phys. Rev. B **45**, 1107 (1992).
[34]C. Jacobini and L. Reggiani, "The Monte Carlo method for the solution of charge transport in semiconductors with applications to covalent materials," Rev. Mod. Phys. **55**, 645 (1983).
[35]E. Gaubasa and J. Vanhellemont, "Dependence of carrier lifetime in germanium on resistivity and carrier injection level," Appl. Phys. Lett. **89**, 42106 (2006).
[36]G. G. Malliaras, J. R. Salem, P. J. Brock, and J. C. Scott, "Photovoltaic measurement of the built-in potential in organic light emitting diodes and photodiodes," J. Appl. Phys. **84**, 1583 (1998), see https://pubs.aip.org/aip/jap/article-pdf/84/3/1583/6751493/1583_1_online.pdf.